Passive Control of Piston Secondary Motion using Nonlinear Energy Absorbers

N. Dolatabadi

Research Associate, Wolfson School of Mechanical, Electrical and Manufacturing Engineering, Loughborough University, Loughborough, LE11 3TU, UK

N.Dolatabadi@lboro.ac.uk

S. Theodossiades

Professor of Nonlinear Dynamics, Wolfson School of Mechanical, Electrical and Manufacturing Engineering, Loughborough University, Loughborough, LE11 3TU, UK

S.Theodossiades@lboro.ac.uk

S. J. Rothberg

Professor of Vibration Engineering and Pro-Vice Chancellor Research, Wolfson School of Mechanical, Electrical and Manufacturing Engineering, Loughborough University, Loughborough, LE11 3TU, UK

S.J.Rothberg@lboro.ac.uk

Abstract

The impulsive behaviour of the piston in the cylinder liner plays a key role in the Noise, Vibration and Harshness (NVH) of internal combustion engines. There have been several studies on the identification and quantification of piston impact action under various operation conditions. In the current study, the dynamics of the piston secondary motion are initially explored in order to describe the aggressive oscillations, energy loss and noise generation. The control of piston secondary motion (and thus, impacts) is investigated using a new passive approach based on energy transfer of the highly transient oscillations to a nonlinear absorber. The effectiveness of this new method for improving the piston impact behaviour is discussed using a preliminary parametric study that leads to the conceptual design of a nonlinear energy absorber.

Key words: Piston secondary motion, Targeted Energy Transfer, Nonlinear Energy Sink, Piston impacts

Introduction

Concerns about traffic noise in urban areas have recently increased. Legislative committees globally are developing strict regulations [1], forcing automotive manufacturers to develop quieter transportation, since the noise originating from the internal combustion engine at low speeds is mainly related to urban driving conditions [2, 3]. Over 33% of the engine mechanical losses are dissipated through the piston-cylinder conjunction in the form of friction, vibrations and noise [4]. Although vibration and noise account for the smallest contribution of losses through the piston skirt and rings, the radiated noise levels are comparable to those from combustion noise. Thus, piston impacts and combustion are the main contributors with their cumulative share representing about 80% of the total engine noise output [5].

The piston impact noise is generated by the impulsive loads due to the secondary motion of the piston (translation and rotation) inside the piston-cylinder clearance. These motions are driven by the cylinder pressure fluctuations, which can be measured accurately using pressure sensors [6, 7]. Analytical and numerical tools have been developed during the past decades to describe the secondary dynamics of the piston. The piston impact problem comprises the piston secondary motion dynamics, the lubrication of the contacting surfaces and their structural deformations. The early studies concentrated mainly on the dynamics [8, 9]. In more advanced piston models, structural deformation and the lubricant's cushioning effects are described using stiffness and damping elements ('dry' models) [10-14]. The parameters of these elements are evaluated either experimentally [15, 16] or theoretically [13]. Models combining tribology and dynamics take into account jointly the effects of piston dynamics, structural deformability and hydrodynamics of the lubricant film (Elasto-hydrodynamic lubrication) [17-19]. Thus, tribodynamics models are largely exploited to predict and identify piston-cylinder interactions [20, 21]. The 'dry models', however, are very useful for extensive parametric studies of the influential factors on the piston secondary motion due to their computational efficiency [22, 23] and reasonably good accuracy [24].

The piston secondary motion is influenced by the engine operating conditions and the geometrical and physical characteristics of the piston assembly components. Piston impacts are conventionally controlled through the modification of component geometry and position. The most influential factors are: the location of the piston's centre of gravity, piston pin offset, piston-cylinder clearance, piston skirt stiffness and crankshaft offset [23, 25-29]. The improvement in NVH performance through those factors can, however, exacerbate friction losses [28, 29]. Thus, a trade-off is usually required between friction loses and NVH. Moreover, these modifications (e.g. crankshaft offset and clearance size) are only effective in specific engine speed ranges [26]. An alternative control method that is robust with engine speed variations should be sought to limit excessive impact excitations more effectively.

The concept of Targeted Energy Transfer (TET) has been introduced in dynamic systems relatively recently. This phenomenon takes place between a (usually) linear primary system and an essentially nonlinear attachment with relatively small mass/inertia (compared to the primary system). The nonlinear device captures part of the unwanted vibration energy from the primary system, which is then either dissipated through weak linear damping or transferred from lower to higher frequency modes, where the damping factor is higher (figure 1). Early studies focused on linear primary systems that are weakly coupled with nonlinear components [30, 31]. These systems are excited by transient (impulsive) forcing [33]. In recent studies, external periodic excitation of the primary system has been investigated in conjunction with nonlinear energy absorbers [32-35]. The TET concept has also been applied to nonlinear primary systems with self-excited instabilities in fluid-structure interactions and stick-slip vibrations [36-39]. Despite the recent trend towards the application of nonlinear energy absorbers to highly transient and nonlinear dynamics of rotational systems [40-43], their application in automotive powertrains is very novel [44]. In this paper, the TET concept is applied to passively control piston secondary motion and reduce the corresponding impacts against the cylinder liner.

The piston dynamics model

'Dry' piston dynamics models are popular for optimization and parametric studies of design variables due to their computational efficiency. The structure and lubricant properties are described through stiffness and damping elements (figure 2). Hertz's theory [45] is a straightforward approach to estimate the stiffness (through compliance) of contacting bodies [14]. The parameters of interest in Hertzian contacts are: the size of the contact area, the pressure developed and the deflection of the contacting bodies. The load (W) and deflection (δ) for circular contact deformation are related as follows:

$$W = \frac{4}{3} E \sqrt{R} \delta^{3/2} = k_{Hertz} \delta^{3/2} \quad (1)$$

E, R and k_{Hertz} are the reduced modulus of elasticity, reduced radius of counter-formal contact and stiffness coefficient of the contact, respectively. There are two sources of energy dissipation at the piston-cylinder conjunction: (i) structural damping and (ii) lubricant damping. The cylinder liner is made of Aluminium in the single-cylinder four-stroke Honda CRF 450 engine that will be the subject of this study. The damping ratio of Aluminium varies between 0.0001 and 0.01

with geometry, acceleration and excitation frequency [46, 47]. For six- and four-cylinder diesel engines the structural damping ratio reportedly varies between 0.01 and 0.0378 [10, 13]. Since the material, size and geometry of these engines are different from the studied one in this work, an indicative structural damping ratio of 0.01 has been selected for the current investigation. The damping effect of the lubricant is neglected for computational efficiency [22]. Thus, the contact load is fully described by taking into account both stiffness and damping terms:

$$W = k_{Hertz}\delta^{3/2} + c_{Hertz}\dot{\delta} \tag{2}$$

The accuracy of the 'dry' piston impact model should be investigated prior to running extensive simulations that will determine the design of the nonlinear absorber. The real contact between piston and cylinder undergoes elasto-hydrodynamic regime of lubrication (EHL). The 'dry' impact model differs from the real piston impact conditions due to the following reasons: (a) In the conformal contact of the real system, deformations take place over the whole piston skirt area (the deformations are localised at the piston corners in the Hertz contact model) and (b) the damping effect of the oil film is neglected and dry contact conditions are assumed. Thus, in the 'dry' model, the piston skirt experiences larger deformations during the combustion stroke. In addition, due to the lack of lubricant's effect the piston can move freely inside the clearance. This motion is more restricted in the real system due to the presence of lubricant. Nevertheless, Offner [24] compared the more realistic EHL contact models against the 'dry' contact model for piston's secondary motion. They reported that the predicted piston secondary motion varies from extremely good to reasonably good during the transition from the EHL model to the 'basic' dry contact model. Thus, the trade-off between the accuracy and computational efficiency is deemed as acceptable [24].

The equations of piston secondary motion

The following equations of motion are widely exploited in the literature with small differences in the notation and coordinate systems:

$$\begin{bmatrix} m_{pis}\left(1-\frac{b}{L}\right)+m_{pin}\left(1-\frac{a}{L}\right) & m_{pis}\frac{b}{L}+m_{pin}\frac{a}{L} \\ \frac{I_{pis}}{L}+m_{pis}(a-b)\left(1-\frac{a}{L}\right) & -\frac{I_{pis}}{L}+m_{pis}(a-b)\frac{b}{L} \end{bmatrix}\begin{Bmatrix}\ddot{e}_t \\ \ddot{e}_b\end{Bmatrix}=\begin{Bmatrix} W \mp F_f \tan\phi - F_t \\ M_W + M_f + M_s \end{Bmatrix} \quad (3)$$

m_{pis}, m_{pin} and I_{pis} are masses of the piston and pin, as well as the inertia of the piston about its centre of rotation. The coordinate system for these equations is depicted in figure 3. The displacements at the top and bottom of the piston skirt are depicted by eccentricities (e_t and e_b). Other geometric parameters are defined in the same figure. The piston side force (F_t) is determined by:

$$F_t = \left(-m_{pin}\ddot{x} - m_{pis}\ddot{x} + F_G \mp F_f\right)\tan\phi \quad (4)$$

The lubricant viscous friction (F_f) and its generated moment (M_f) are neglected as their influence on the impact force is less than 3% [48]. M_W is the moment due to the contact load (W) about the piston pin. M_s describes the moment due to combustion and piston inertia forces (offsets) with respect to the piston pin centre of rotation. This parameter is trivial as offsets equal zero for the examined engine. For detailed description of the equations of motion the reader may refer to [20, 21].

The results of the piston model are validated against the work of Offner [24] for 'dry' contact conditions (figure 4). It should be noted that the operating conditions and engine characteristics are different in those models. Moreover, Offner [24] employs FEM to extract the stiffness properties of the contacting bodies. One should also note that Offner [24] has reported the gap size (C_t and C_b at the TS and ATS sides) whereas the piston dynamics model in this study uses the cylinder's axis as the reference for the piston displacement (eccentricities e_t and e_b). Thus, only qualitative comparison of the results is possible. Offner's model overestimates the gap sizes at the bottom land towards the bottom dead centres, since this model does not generate any balancing force in this free-motion period [24]. In other parts of the engine cycle, good conformity is observed between the events in both models. In both models, the piston stays at the thrust side during combustion stroke due to the large side force. The piston is moving more inside the clearance during the exhaust and intake strokes, since the side forces are smaller in the absence of significant cylinder pressure. Six side-to-side piston translations are present in both models, related to piston impacts. The (crank) angular positions of these translations inside the engine cycle conform well in both models. In addition, the eccentricity displacements are in the

proximity of the clearance size ($\pm 18\ \mu m$ for the proposed piston model). The mentioned features verify that the piston model is compatible with the physics of the problem.

Nonlinear energy absorber design considerations

The nonlinear energy absorber comprises low inertia/mass and an element of essential nonlinear stiffness and weak, linear damping. The nonlinearity facilitates the interaction with the primary system between different structural modes that are either closely located or well-separated. These nonlinear modes are excited due to internal resonances, which enable the absorber to engage with the primary system. Provided the input energy to the absorber is localised to a specific frequency range, the nonlinear absorber initiates an internal resonance with the main system. Once the dynamics is established, energy is transferred from the primary system to the nonlinear absorber in an irreversible fashion. The obtained energy dissipates in the absorber through the damping element. The above mechanism is known as targeted energy transfer (TET) [30].

In order to apply the TET concept to a piston system, the proposed nonlinear absorber design should be robust to system uncertainties, initial conditions and external excitations. In the piston assembly, the excitation frequency is expressed in terms of the engine firing orders. Combustion excitations are related to half engine orders (in four-stroke engines) and mechanical excitations (piston impact, bearings etc.) appear at multiples of the engine orders [49]. The piston secondary motion also contains these dominant frequencies in its spectra (figure 5). The inertial forces are dominant at 50 Hz (1st engine order at 3000 rpm engine speed). The spectral amplitude of the rotational motion is one order of magnitude greater than that of the translational motion at the first engine order. This behaviour suggests that an absorber with rotational motion might effectively remove the excess impact energy.

A pendulum mechanism (illustrated in figure 6) is proposed to rotate about the piston pin, reacting to piston rotation through a torsional spring with cubic nonlinearity and a weak torsional linear damper. The main assumptions employed in this design are:

1. The pendulum has a lumped mass (m_t) located at its free end
2. The masses of the link, spring and damper are negligible
3. Both piston and pendulum are aligned with the cylinder axis at the equilibrium position
4. There is no friction or clearance between the pendulum and either the piston or the piston pin

The pendulum design parameters for the purpose of this study are the following: the spring constant of stiffness (k_t), damping constant (c_t), mass (m_t) and length (L_t). These parameters influence the absorber's angular oscillations (γ).

It has to be noted that although a frictionless conjunction between the pendulum and the piston components cannot be fully achieved, this assumption is not far from reality since lubrication can reduce friction on this contact. The shear

action of the lubricant can be readily exploited as an internal source of damping for the nonlinear absorber. On the other hand, the design of a nonlinear torsional spring element requires a separate study that will investigate the relevant practicalities in depth. Nevertheless, a few designs are patented for nonlinear torsional springs [50] and could be tailored for engine applications. The stiffness linearity is expected to influence the absorber's performance negatively, since it will prevent the communication between the primary system and the absorber under nonlinear resonance capture.

Piston dynamics with the nonlinear absorber

The piston and nonlinear absorber reaction forces and moments are presented in the corresponding free body diagrams (figure 7). The reaction forces at the pin location are $F_{t,z}$ and $F_{t,x}$ and the reaction moment of the absorber's spring and damper are depicted by M_t. The piston motion is coupled with the pendulum absorber through these forces and moment. The contact forces are located at the four corners of the piston skirt ($F_{H,A}$ and $F_{H,C}$ at the thrust side and $F_{H,B}$ and $F_{H,D}$ at the anti-thrust side). These forces are evaluated using equation (2). The other forces, moments and geometrical parameters are the same as in equations (3) and (4). The kinematics of the pendulum are shown in figure 8 and the relation with piston kinematics is described through:

$$\begin{aligned} x_t &= x + L_t \cos\gamma \\ \ddot{x}_t &= \ddot{x} - L_t\ddot{\gamma}\sin\gamma - L_t\dot{\gamma}^2\cos\gamma \\ z_t &= z - L_t \sin\gamma \\ \ddot{z}_t &= \ddot{z} - L_t\ddot{\gamma}\cos\gamma + L_t\dot{\gamma}^2\sin\gamma \end{aligned} \tag{5}$$

The above kinematic relations are exploited in the derivation of the equations of motion. Three sets of equations describe the system dynamics:

$$\boldsymbol{M}_{3\times3}\begin{Bmatrix}\ddot{e}_t \\ \ddot{e}_b \\ \ddot{\gamma}\end{Bmatrix} = \begin{Bmatrix} F \\ M_1 \\ M_2\end{Bmatrix} \tag{6}$$

The elements of the inertia ($\boldsymbol{M}_{3\times3}$) and force matrices are provided below:

$$
\begin{aligned}
m_{11} &= m_{pis}\left(1-\frac{b}{L}\right)+\left(m_{pin}+m_t\right)\left(1-\frac{a}{L}\right)\\
m_{12} &= m_{pis}\frac{b}{L}+\left(m_{pin}+m_t\right)\frac{a}{L}\\
m_{13} &= -m_tL_t(\cos\gamma+\sin\gamma\tan\phi)\\
m_{21} &= \frac{I_{pis}}{L}+m_{pis}(a-b)\left(1-\frac{a}{L}\right)\\
m_{22} &= -\frac{I_{pis}}{L}+m_{pis}(a-b)\left(1-\frac{a}{L}\right)\\
m_{23} &= 0\\
m_{31} &= -m_tL_t\left(1-\frac{a}{L}\right)\cos\gamma\\
m_{32} &= -m_tL_t\frac{a}{L}\cos\gamma\\
m_{33} &= m_tL_t^2
\end{aligned}
\tag{7}
$$

$$
\begin{aligned}
F &= \left(-F_G+\left(m_{pin}+m_{pis}+m_t\right)\ddot{x}\right)\tan\phi-\left(m_tL_t\dot{\gamma}^2\cos\gamma+m_tg\right)\tan\phi-m_tL_t\dot{\gamma}^2\sin\gamma+\sum F_{H,i}\\
M_1 &= M_t+M_H+M_f+M_s\\
M_2 &= -M_t-m_tL_tg\sin\gamma+m_tL_t\ddot{x}\sin\gamma
\end{aligned}
\tag{8}
$$

The pendulum mass is commonly expressed as a percentage of the mass ratio (the absorber mass over the mass of the primary system, which is the total mass of the piston and pin in this case). $F_{H,i}$ represents the Hertzian contact forces at the four piston corners as described earlier ($i = A, B, C$ and D). M_H is the overall moment about the piston pin due to these contact forces. The pendulum moment (M_t) is described as:

$$M_t = k_t(\gamma-\beta)^3+c_t(\dot{\gamma}-\dot{\beta}) \tag{9}$$

β is the piston rotation about its pin and it can be defined in terms of piston eccentricities (e_t and e_b) [19]. Newmark integration and predictor-corrector techniques are exploited to numerically solve equations (6).

The effectiveness of the nonlinear absorber (in the 3 degree of freedom piston – absorber system, 3dof) in mitigating piston impacts is explored in comparison with the primary 2 degree-of-freedom (2dof) piston system (nonlinear absorber not present) using the following piston impact criteria: (i) piston impact severity (eccentricity accelerations), (ii) number of impacts and (iii) transferred energy to the cylinder liner. The first two criteria represent the impact behaviour at the source; whereas, the last criterion indicates the effect of impact on the structure. The percentages of variations in these criteria are evaluated as:

$$\%\Delta V = \frac{V_{2dof} - V_{3dof}}{V_{2dof}} \times 100 \tag{10}$$

V can be replaced by the variables of each criterion (e.g. eccentricity acceleration $\ddot{e}_t$ for the severity criterion at the piston top land). Positive variations signify improvement and negative values indicate exacerbation in that criterion. The transferred energy to the cylinder liner is calculated over a complete engine cycle for both the thrust and anti-thrust sides of the structure as follows (t and b indicate top and bottom of the piston skirt and W is calculated from equation (2) :

$$ET = \oint W_t d\delta_t + \oint W_b d\delta_b \tag{11}$$

The simulation time step is invariable, equal to 5 μs. This low value was chosen after trial simulations because of the fast nature of the examined vibro-impact problem. The convergence criterion is 1%, implemented on the accelerations ($\ddot{e}_t$, $\ddot{e}_b$ and $\ddot{\gamma}$), which are the fastest system variables. The kinematics of the piston and the absorber are evaluated using Newmark's integration method [51] for dynamic systems. This method is also known as the average acceleration method [52].

Ranges of values (due to commercial confidentiality) of the system parameters used in the simulations are provided in the table below. The ranges of the parametric studies are described in the results section.

Table 1. Ranges of values of the system parameters utilised during simulations

Parameter	Value	Unit
$m_{pis} + m_{pin}$	0.25 – 0.4	Kg
m_t	0.125 $(m_{pis} + m_{pin})$	Kg
I_{pis}	$1.5\times10^{-4} - 3\times10^{-4}$	$Kg.m^2$
a	0.015 – 0.03	m
b	0.008 - 0.02	m
L	0.03 – 0.05	m
L_t	0.04 – 0.06	m
k_H	60 – 80	$GN/m^{1.5}$
ζ_H	0.005 – 0.02	--

Results and discussion

The conventional methods for mitigating piston impacts are usually effective at specific engine speed ranges. The TET concept is proposed as an alternative that can perform robustly across the full speed range. The energy content of impacts generally increases with engine speed. Moreover, speed fluctuations due to cylinder pressure variations can influence the impact characteristics. For this purpose, engine speed fluctuations are measured at three different engine speeds from a test-rig with fired engine conditions (figure 9). The other engine speed conditions are interpolated using a Lagrange interpolator. Measurements are carried out using a Honda CRF 450R single cylinder, 4-stroke motorbike SI engine. The engine is resisted by an Oswald 250 kW transient dynamometer and is controlled to the desired speeds by the installed Ricardo Software. The crank position is detected through an optical reader, which records 360 pulses in each complete crank rotation and detects a single TDC pulse. The crank speed is calculated using crank angle and time data. The output signals are input to a LabVIEW programme and post-processed for the simulations. Detailed description of the experimental setup is given in the previous works of the authors [20, 21]. The in-cylinder pressure, engine speed and crank angle time histories are measured in the Honda CRF450 engine. The in-cylinder pressure is

exploited to evaluate the combustion force. The engine speed is utilised in the calculation of piston kinematics in its primary direction. The crank angle information is used to synchronise the measured and calculated data. These parameters are the essential model inputs and they are used to generate the simulation results.

The mean engine speed increases between 3000 - 4200 rpm in 200 rpm steps. Initially, the damping coefficient and pendulum length are held constant (0.01 Nms/rad and 0.05 m). The pendulum has 12.5% mass ratio. The stiffness coefficient of the nonlinear absorber varies between 10 and 110 (Nm/rad^3). The percentage of variation in impact severity criterion is illustrated in the contour maps of figure 10. These variations are calculated using equation (10). The eccentricity accelerations are generally improved at both the top and bottom of the piston skirt. The robustness of the absorber with respect to its damping coefficient and engine speed variations is investigated in figure 11. The stiffness constant is set to 40 (Nm/rad^3) for this study whereas the damping coefficient varies between 0 and 0.045 (Nms/rad). The eccentricity accelerations (impact severity) are improved by up to 20% at the top of the piston skirt. Energy dissipation effectively takes place for damping coefficient values between 0.01 and 0.015 (Nms/rad). Since the absorber performance shows robustness with engine speed in both scenarios, a single speed suffices for the study of the absorber's influence on the piston impact criteria.

For the parametric study that follows (aiming to identify the best performing absorber characteristics) the engine speed is set to 3500 rpm since the absorber has exhibited robust behaviour with respect to engine speed. The mass ratio and pendulum length are held constant (12.5% and 0.05 m, respectively). The absorber is tuned to piston excitations through the variation of its stiffness coefficient between 10 and 110 Nm/rad^3. Since energy dissipation is as important as tuning, the damping coefficient is varied between 0 and 0.045 Nms/rad. The different piston impact criteria are illustrated through contour maps in figures 12 to 14.

The impact severity criterion is the most significant factor in assessing the likely improvement in piston impact noise levels, since it captures the eccentricity accelerations for the severe impact events of the engine cycle (including combustion). These accelerations noticeably improve (up to 20%) as damping coefficient approaches 0.01 Nms/rad (figure 12). This trend reverses as damping coefficient increases to values greater than 0.02 Nms/rad, indicating that the nonlinear energy absorber operates more effectively with low damping. The number of impacts criterion comes secondary to impact severity in terms of importance, since more impacts with lower severity are preferable to fewer impacts with higher severity. The number of impact events generally reduces up to 25% at the top eccentricity for damping coefficient values between 0.01 and 0.02 Nms/rad (figure 13). At the bottom eccentricity, the observed 25% exacerbation in the number of events reduces to 0% as the damping coefficient increases from 0.01 to 0.02 Nms/rad.

Although impact severity largely improves for damping 0.01 Nms/rad, the overall number of impacts is invariant. 25% improvement in the number of impacts at the top eccentricity cancels out with 25% exacerbation at the bottom eccentricity for this damping condition. The impact severity improves to a smaller extent for damping 0.02 Nms/rad and stiffness values greater than 90 Nm/rad^3. For these stiffness and damping values, the number of impacts also improves up to 25%.

The third criterion indicates the overall transferred energy to the cylinder liner during an engine cycle (figure 14). This ensures that the deployment of the absorber also reduces the amount of energy transferred to the cylinder. The energy transfer criterion excessively exacerbates in a small area for zero damping and low stiffness conditions. This area though is not influential in the design of the absorber. The energy transfer variations are not large in most part of the figure since they are calculated over the entire engine cycle and impact events only occupy a small fraction of the cycle. For a damping coefficient value of 0.01 Nms/rad, two regions of stiffness coefficient satisfy the reduction in energy transfer criterion (stiffness values about 65 Nm/rad^3 and values greater than 90 Nm/rad^3). The energy transfer criterion returns slightly worse results for stiffness values greater than 90 Nm/rad^3 and 0.02 Nms/rad damping coefficient. The proposed nonlinear absorber successfully mitigates the impact severity, whilst the overall transferred energy through the contact and the number of impacts are invariant (figures 12 to 14). There is potential to improve the number of impacts through the optimization of the absorber design whilst there is potential for a trade-off between impact severity and impact number criterion.

Based on the above simulation results an indicative pendulum absorber design was selected for detailed performance analysis. The stiffness and damping coefficients were taken as 65 Nm/rad^3 and 0.01 Nms/rad for this design. Figure 15 illustrates the hysteresis loop of the pendulum oscillations. The stiffness moment takes values up to 12 times higher than the damping moment, exhibiting the action of the absorber. Figure 16 compares the eccentricity accelerations at the top and bottom of the piston skirt ($\ddot{e}_t$ and $\ddot{e}_b$) for the 2dof and 3dof systems. The graphs are presented for three engine cycles to show the stability of the simulation results. The acceleration (impact severity) is largely mitigated at the bottom eccentricity in the presence of the pendulum (3dof). The minimum acceleration is noticeably reduced at the top eccentricity, whilst the maximum acceleration improves to a smaller extent.

The number of impacts can be identified using the time histories of the eccentricity displacements (e_t and e_b in figure 17). The pendulum eliminates two impacts at the top eccentricity during each engine cycle (labels A and B), whilst two impacts appear at the bottom eccentricity during the compression stroke (e.g. labels C and D during 540 to 720° crank

angle). Although the total number of impacts has not changed, the impulsive nature of the impacts has improved through the mitigation of eccentricity accelerations.

The time histories of the piston secondary motions (translation e_p and rotation β) and pendulum angular oscillations (γ) are presented in figure 18. The rotation of piston has increased during the intake stroke (e.g. 360 to 540° crank angle), mitigating the piston's translation. The piston rotational displacement is also slightly mitigated during the combustion stroke (about 14° crank angle). The piston moves to the centre of the clearance during the compression mid-stroke (-90° crank angle). The impact is then related to pure rotation of the piston in this instance. The pendulum absorber completes one oscillation every engine cycle. Its oscillation amplitude is naturally restricted to the physical boundaries of the cylinder liner. Thus, the pendulum mass does not impinge against the cylinder liner. The frequency spectra of the above mentioned displacements explain the communication between the pendulum and piston secondary motions (figure 19). In the absence of the nonlinear absorber (figure 5), the piston translation and rotation are dominant at the first and second engine orders. In the presence of the pendulum, the spectral amplitude of piston translation is still dominant at the first and second engine orders (figure 19). However, the difference between the amplitudes at the first and second engine orders (58 and 116 Hz) and the half and 1.5 engine orders (29 and 87 Hz) decreases remarkably. In the case of piston rotation, the spectral amplitudes generally increase and the half and first engine orders become equally dominant. The piston rotation is the primary drive for pendulum oscillations since its spectral amplitudes are one order of magnitude greater than piston translation and the pendulum's FFT content coincides with the dominant frequencies in piston rotation.

Conventionally, the piston-skirt impact noise (slapping) is controlled by modifying parameters affecting piston's secondary motion, such as the clearance size, piston skirt profile, piston skirt stiffness, piston pin offset and the crankshaft offset [53]. Although improvements on piston noise can be achieved using these methods, other characteristics of the system's performance can be negatively affected, such as friction loss and blow-by [53]. For instance, smaller clearance size improves the impact noise behaviour in spite of the increased friction loss [28, 29]. Nakayama [26] proves that the effectiveness of the crankshaft offset reduces at high engine speeds. The nonlinear absorber's performance is, however, robust with engine speed variation. Thus, the proposed nonlinear absorber has a potential in controlling piston's secondary motion.

Conclusions

Piston secondary motion is the main cause of impact noise in internal combustion engines. Conventional control methods to mitigate this issue are effective only in certain ranges of the engine operating conditions. The aim of this paper is to present a study based on the TET concept that has the potential to lead to improved impulsive behaviour of the piston against the cylinder liner as a more robust passive control tool for the transient nonlinear system under examination. The following conclusions are made through this research:

- The piston rotation is the most influential parameter for piston impact severity. Absorber designs should initially target piston rotation.
- The crankshaft offset, piston-pin offset and clearance size are the three main conventional methods to control piston impacts. Even though modifying crankshaft offset seems to be the best approach, its implementation is expensive and its effectiveness decays as the engine speed increases. The examined TET concept is robust to engine speed variation and it can strongly influence the piston's secondary motion. This robustness is maintained across a broad range of pendulum (nonlinear) stiffness and damping coefficients.
- The proposed nonlinear absorber successfully mitigates the impact severity, whilst the overall transferred energy through the contact and the number of impacts are rather invariant during the entire engine cycle. For the examined design (stiffness-damping combination), the damping element produces moments of more than one order of magnitude less than those of the absorber's stiffness action. This ratio signifies that the damping element is sufficiently weak for the selected TET design.
- It is shown that there is potential to simultaneously improve the number of impacts provided the absorber design is optimised and a trade-off is acceptable in impact severity. An optimization study, considering use of more than one nonlinear absorber, is proposed for future work.

Acknowledgments

The authors wish to express their gratitude to the EPSRC for the financial support extended to the Encyclopaedic Program Grant (EP/G012334/1), under which this research was carried out. Thanks are also due to the consortium of industrial partners of the Encyclopaedic project, particularly to Capricorn Automotive in this instance.

References

[1] "Regulation (EU) No 540/2014 of the European Parliament and of the Council of 16 April 2014 on the sound level of motor vehicles and of replacement silencing systems, and amending Directive 2007/46/EC and repealing Directive 70/157/EEC Text with EEA relevance," OJ L 158, 27.5.2014, p. 131–195.

[2] Rahnejat, H., 2000, "Multi-body dynamics: historical evolution and application," Proc. Ins. Mech. Eng.: Part C, **214**, pp. 149-173.

[3] Gupta, S., 2002, "Elasto-multi-body dynamics of internal combustion engines with thin shell elastohydrodynamic journal bearings," PhD Thesis, Loughborough University.

[4] Rahnejat, H., 2010, *Tribology ad dynamics of engine and powertrain: Fundamentals, applications and future trends*, Woodhead Publishing Ltd., Chapter 10.

[5] Kanda, H., Okubo, M., and Yonezawa, T., 1990, "Analysis of noise sources and their transfer paths in diesel engines," SAE International, SAE900014.

[6] Chen, L., and Mehregany, M., 2008, "A silicon carbide capacitive pressure sensor for in-cylinder pressure measurement," Sensors and Actuators: A, **145-146**, pp. 2-8.

[7] Litak, G., Taccani, R., Radu, R., Urbanowicz, K., Holyst, J.A., Wendeker, M., and Giadrossi, A., 2005, "Estimation of a noise level using coarse-grained entropy of experimental time series of internal pressure in a combustion engine," J. Chaos, Solitons and Fractals, **23**, pp. 1695-1701.

[8] Ungar, E.E., and Ross, D., 1965, "Vibration and noise due to piston-slap in reciprocating machinery," J. Sound and Vibration, **2**(2), pp. 132-146.

[9] Haddad, S.D., and Howard, D.A., 1980, "Analysis of piston slap-induced noise and assessment of some methods of control in diesel engine," SAE technical paper, SAE800517.

[10] Haddad, S.D., and Fortescue, P.W., 1977, "Simulating piston slap by an analogue computer," J. Sound and Vibration, **52**(1), pp. 79-93.

[11] Lalor, N., Grover, E.C., and Priede, T., 1980, "Engine noise due to mechanical impacts at pistons and bearings," SAE Technical Paper, SAE800402.

[12] Nakada, T., Yamamoto, A., and Abe, T., 1997, "A numerical approach for piston secondary motion analysis and its application to the piston related noise," SAE Technical Paper, SAE972043, pp. 1361-1370.

[13] Cho, S.H., Ahn, S.T., and Kim, Y.H., 2002, "A simple model to estimate the impact force induced by piston slap," J. Sound and Vibration, **255**(2), pp. 229-242.

[14] Ohta, K., Amano, K., Hayashida, A., Zheng, G., and Honda, I., 2011, "Analysis of piston slap induced noise and vibration of internal combustion engine (effect of piston profile and pin offset)," J. Environment and Engineering, **6**(4), pp. 765-777.

[15] Geng, Z., and Chen, J., 2005, "Investigation into piston-slap induced vibration for engine condition simulation and monitoring," J. Sound and Vibration, **282**, pp. 735-751.

[16] Gerges, S.N.Y., De Luca, J.C., and Lalor, N., 2002, "The influence of cylinder lubrication on piston slap," J. Sound and Vibration, **257**(3), pp. 527-557.

[17] Zhu, D., Cheng, H.S., Arai, T., and Hamai, K., 1992, "A numerical analysis for piston skirts in mixed lubrication – Part I: Basic modelling," J. Trib., Transaction of ASME, **114**, pp. 553-562.

[18] D'Agostino, V., Guida, D., Ruggiero, A., and Russo, A., 2006, "Optimized EHL piston dynamics computer code," *Proc. the 5th International Trib. Conf.*, AITC-AIT, Parma, Italy.

[19] Littlefair, B., De-La-Cruz, M., Theodossiades, S., Mills, R., Howell-Smith, S., Rahnejat, H., and Dwyer-Joyce, R., 2014, "Transient tribo-dynamics of thermos-elastic compliant high-performance piston skirts," Trib. Lett., **53**(1), pp. 51-70.

[20] Dolatabadi, N., Littlefair, B., De-La-Cruz, M., Theodossiades, S., Rothberg, S. J., and Rahnejat, H., 2015, "A transient tribodynamic approach for the calculation of internal combustion engine piston slap noise," J. Sound and Vibration, **352**, pp. 192-209.

[21] Dolatabadi, N., Theodossiades, S., and Rothberg, S. J., 2015, "On the identification of piston slap events in internal combustion engines using tribodynamic analysis," Mech. Sys. and Sig. Proc., **58-59**, pp. 308-324.

[22] Goenka, P.K., and Meernik, P.R., 1992, "Lubrication analysis of piston skirts," SAE Technical paper, SAE920490, pp. 77-86.

[23] Haddad, S.D., and Tjan, K.T., 1995, "An analytical study of offset piston and crankshaft designs and the effect of oil film on piston slap excitation in a diesel engine," Mech. Mach. Theory, **30**(2), pp. 271-284.

[24] Offner, G., Herbst, H.M., and Priebsch, H.H., 2001, "A methodology to simulate piston secondary movement under lubricated contact conditions," SAE technical paper, SAE2001-01-0565, **215**, pp. 93-102.

[25] Nakashima, K., Yajima, Y., and Suzuki, K., 1999, "Approach to minimization of piston slap force for noise reduction – investigation of piston slap force by numerical simulation," SAE of Japan, **20**, pp. 211-216.

[26] Nakayama, K., Tamaki, S., Miki, H., and Takiguchi, M., 2000, "The effect of crankshaft offset on piston friction force in a gasoline engine," SAE technical paper, SAE2000-01-0922.

[27] Li, D.F., Rohde, S.M., and Ezzat, H.A., 1983, "An automotive piston lubrication model," ASLE Trans., **26**(2), pp. 151-160.

[28] Mansouri, S.H., and Wong, V.W., 2005, "Effects of piston design parameters on piston secondary motion and skirt-liner friction," Proc. Inst. Mech. Eng. Part J: J. Eng. Trib., **219**, pp. 435-449.

[29] Offner, G., Lorenz, N., and Knaus, O., 2012, "Piston clearance optimization using thermos-elasto hydrodynamic simulation to reduce piston slap excitation and friction loss," SAE International, SAE2012-01-1530.

[30] Vakakis, A.F., Gendelman, O.V., Bergman, L.A., McFarland, D.M., Kerschen, G., and Lee, Y.S., 2008, *Nonlinear targeted energy transfer in mechanical and structural systems*, Springer Science and Business Media, **156**, ISBN-13: 978-1-4020-9125-4.

[31] Gendelman, O., Manevitch, L.I., Vakakis, A.F., and M'Closkey, R., 2001, "Energy pumping in nonlinear mechanical oscillators: Part I: Dynamics of the underlying Hamiltonian systems," J. App. Mech., **68**, pp. 34-41.

[32] Vakakis, A.F., Manevitch, L.I., Gendelman, O., and Bergman, L., 2003, "Dynamics of linear discrete systems connected to local, essentially non-linear attachements," J. Sound and Vibration, **264**, pp. 559-577.

[33] Gendelman, O.V., and Starosvetsky, Y., 2008, "Quasi-periodic response regimes of linear oscillator coupled to nonlinear energy sink under periodic forcing," J. App. Mech., **74**, pp. 325-331.

[34] Kurt, M., Eriten, M., McFarland, D.M., Bergman, L.A., and Vakakis, A.F., 2014, "Frequency-energy plots of steady-state solutions for forced and damped systems, and vibration isolation by nonlinear mode localization," Communication in Nonlinear Science and Numerical Simulation, **19**, pp. 2905-2917.

[35] Ji, J.C., 2012, "Application of a weakly nonlinear absorber to suppress the resonant vibrations of a forced nonlinear oscillator," ASME, J. Vib. Acoust., **134**(4), doi:10.1115/1.4005839.

[36] Lee, Y.S., Vakakis, A.F., Bergman, L.A., McFarland, D.M., and Kerschen, G., 2007, "Supressing aeroelastic instability using broadband passive targeted energy transfer, Part I: Theory," AIAA Journal, **45**(3), pp. 693-711.

[37] Lee, Y.S., Kerschen, G., McFarland, D.M., Bergman, L.A., and Vakakis, A.F., 2007, "Supressing aeroelastic instability using broadband passive targeted energy transfer, Part II: Experiments," AIAA Journal, **45**(10), pp. 2391-2400.

[38] Viguie, R., Kerschen, G., Golival, J.C., McFarland, D.M., Bergman, L., Vakakis, A., and van de Wouw, N., 2007, "Using targeted energy transfer to stabilize drill-string systems," *The International Modal Analysis Conference XXV*, Orlando, Florida, 19-22 February.

[39] Mehmood, A., Nayfeh, A.H., and Hajj, M.R., 2014, "Effects of a nonlinear energy sink (NES) on vortex-induced vibrations of a circular cylinder," J. Nonlinear Dynamics, **77**(3), pp. 667-680.

[40] Guo, C., Al-Shudeifat, M.A., Vakakis, A.F., Bergman, L.A., McFarland, D.M., and Yan, J., 2015, "Vibration reduction in unbalanced hollow rotor systems with nonlinear energy sinks," J. Nonlinear Dynamics, **79**, pp. 527-538.

[41] Monroe, R.J., and Shaw, S.W., 2013, "Nonlinear Transient Dynamics of Pendulum Torsional Vibration Absorbers – Part I: Theory," ASME, J. Vib. Acoust., **135**(1).

[42] Monroe, R.J., and Shaw, S.W., 2013, "Nonlinear Transient Dynamics of Pendulum Torsional Vibration Absorbers – Part II: Experimental results," ASME, J. Vib. Acoust., **135**(1).

[43] Lee, Y.S., Vakakis, A.F., Bergman, L.A., McFarland, D.M., Kerschen, G., Nucera, F., Tsakirtzis, S., and Panagopoulos, P.N., 2008, "Passive nonlinear targeted energy transfer and its application to vibration absorption: a review," Proc. Inst. Mech. Eng., Part K: J. Multi-Body Dyn., **222**, pp. 77-134.

[44] Dolatabadi, N., Theodossiades, S., Rothberg, S.J., 2015, "Application of nonlinear vibration absorber to the control of piston secondary motion in internal combustion engines," *Proc. ASME., IDETC/CIE*, Boston, Massachusetts, USA.

[45] Hertz, H., 1882, "Über die Berührung fester elastischer Körper (On the contact of elastic solids)," Journal für die reine und angewandte Mathematik, **92**, pp.156-171. (For English translation see *Miscellaneous Papers by H. Hertz*, Eds. Jones and Schott, London: Mcmillan, 1896).

[46] Granick, N., and Stern, J.E., 1965, "Material damping of Aluminium by a resonant-dwell technique," NASA Technical Note, D-2893.

[47] Crawley, E.F., and Van Schoor, M.C., 1987, "Material damping in Aluminium and metal matrix composites," J. Comp. Mat., **21**, pp. 553-568.

[48] Cho, J., and Jang, S., 2004, "Effects of skirt profiles on the piston secondary movements by the lubrication behaviour," International J. Auto. Tech., **5**(1), pp. 23-31.

[49] Rahnejat, H., 1998, *Multi-body dynamics: vehicles, machines and mechanisms*, Professional Engineering Publishing, London, ISBN 9781860581229.

[50] Carvey, M.R., Carvey, A.W., Carvey, P.P., Rokosz, J.A., and Howard, N.S., 2013, "Nonlinear torsion spring assembly" Patent US20130075966, US Patent Application number 13/243,333.

[51] Newmark N.M., 1959, "A numerical method for structural dynamics", Journal of Engineering Mechanics (ASCE), **85**, pp. 67-94.

[52] Timoshenko**,** S., Young, D.H. and Weaver, W., 1974, *Vibration problems in Engineering*, 4th edition, John Whiley and Sons, New York, ISBN 0471873152.

[53] Edara, R., 2008, "Reciprocating engine piston secondary motion – literature review", SAE Technical paper, SAE 2008-01-1045.

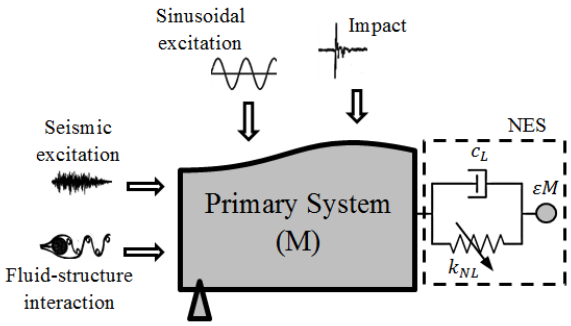

Fig.1. The generic mechanism of passive TET through nonlinear energy sink (NES) [43]

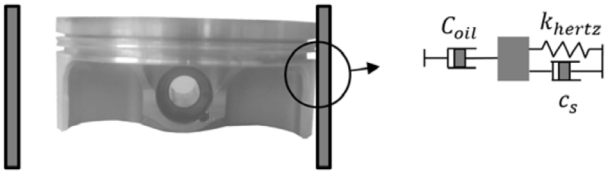

Fig.2. Structure/lubricant property arrangements for the piston dynamics model

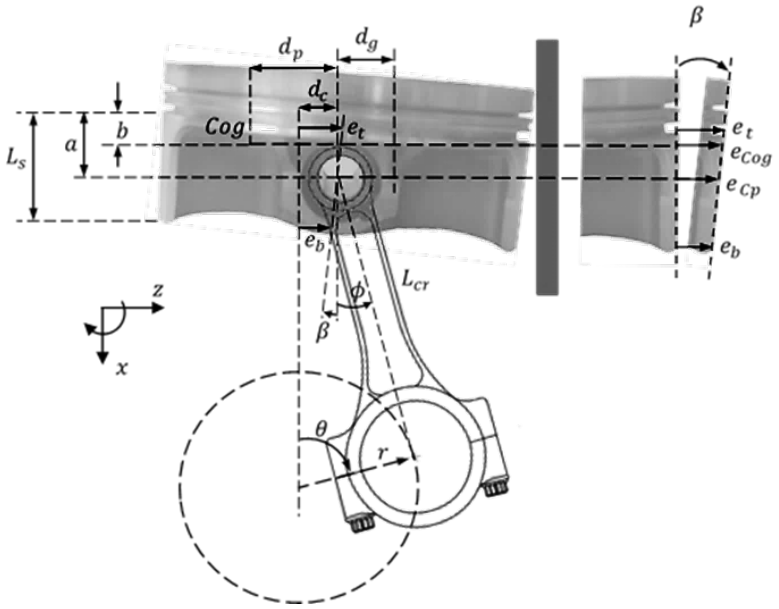

Fig.3. Piston assembly and its geometric parameters

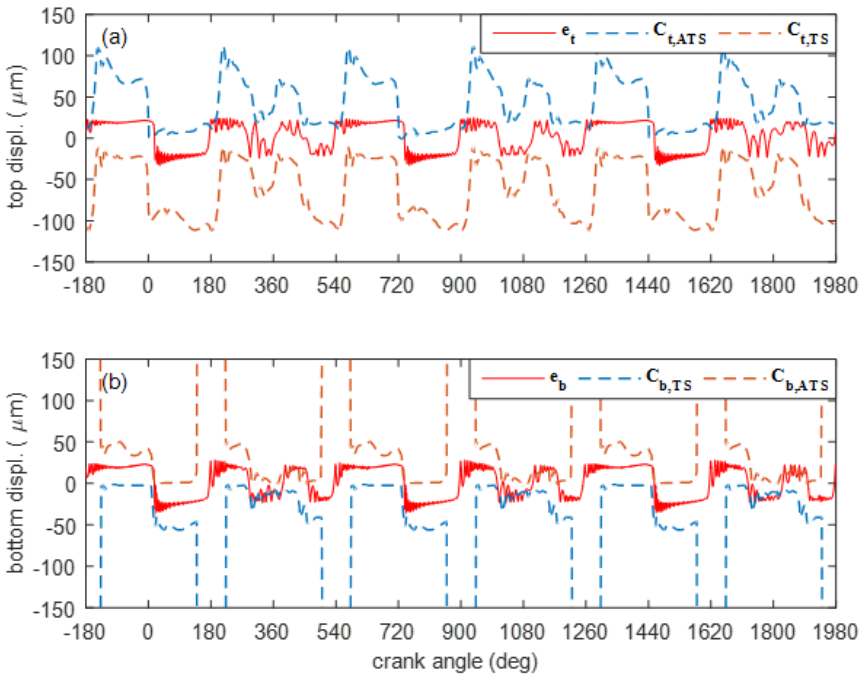

Fig. 4. Piston model validated against a 'dry' contact model by Offner [24]: (a) top and (b) bottom lands of the piston skirt (eccentricity displacements e_t and e_b (with respect to the cylinder centreline), anti-thrust side clearances $C_{t,ATS}$ and $C_{b,ATS}$ (Offner [24]) and thrust-side clearances $C_{t,TS}$ and $C_{b,TS}$ (Offner [24])).

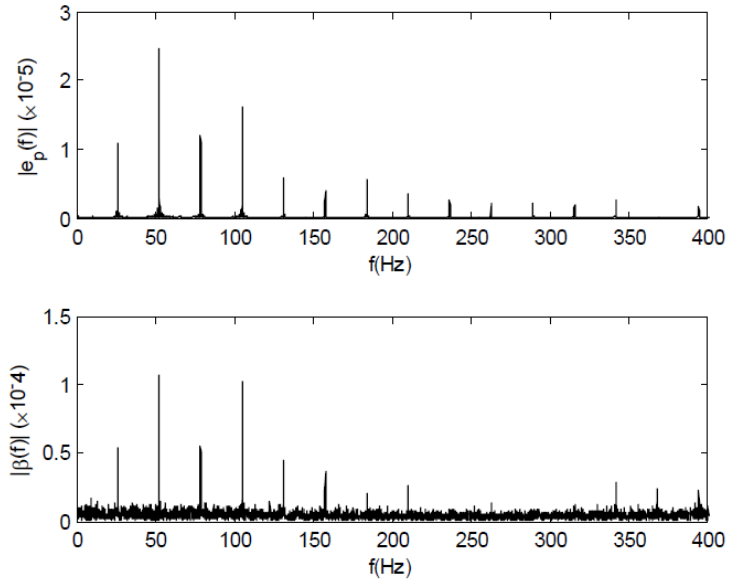

Fig.5. FFT spectra of the piston secondary motions: translation (e_p) and rotation about the piston pin (β).

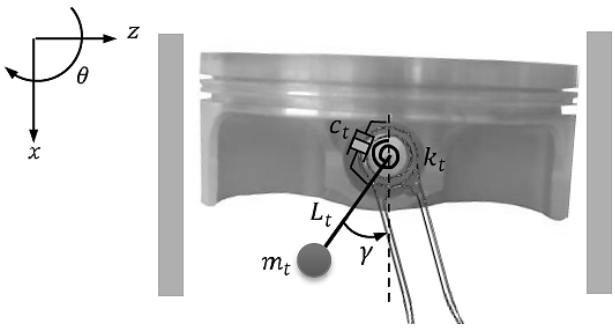

Fig.6. Single pendulum nonlinear energy absorber coupled with the piston assembly

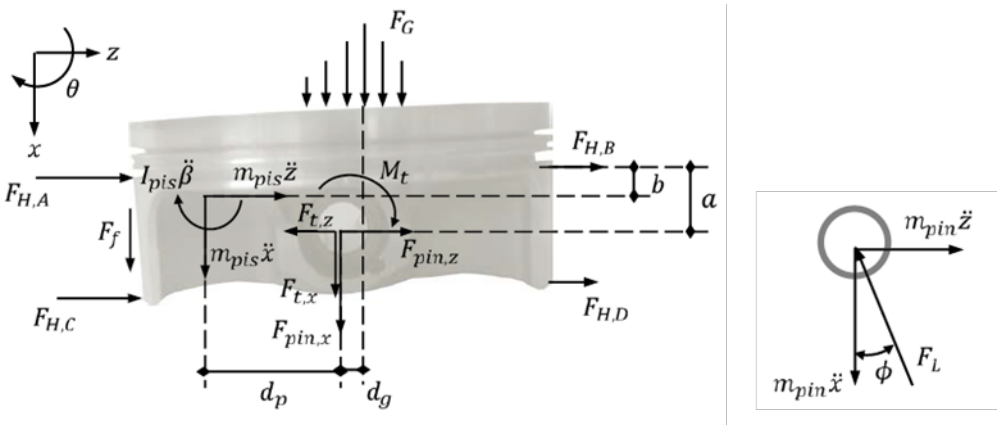

Fig.7. Free body diagrams of the piston and pin, including the absorber reactions

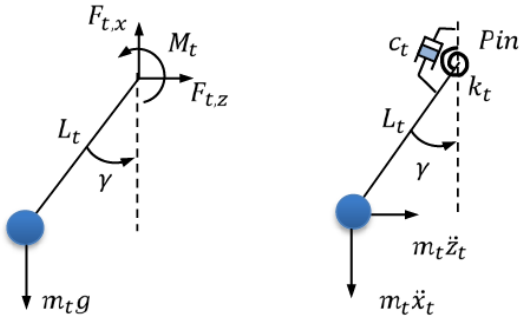

Fig.8. Free body diagram of the pendulum absorber (with left diagram showing external excitations and right diagram depicting the inertial forces)

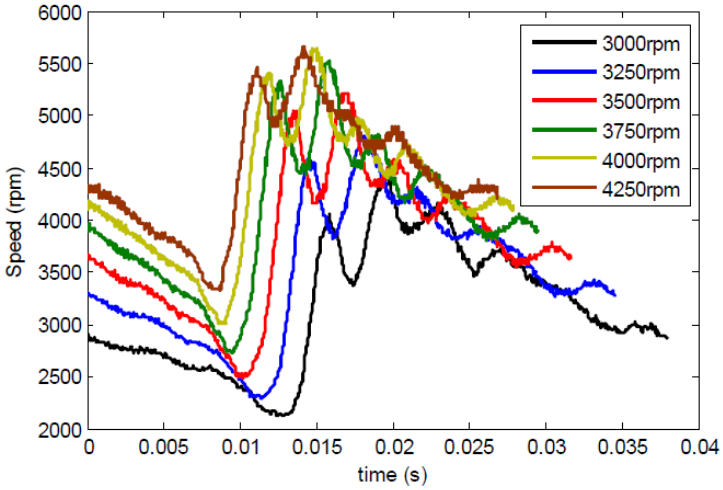

Fig.9. Engine speed variations during one engine cycle for different engine speeds

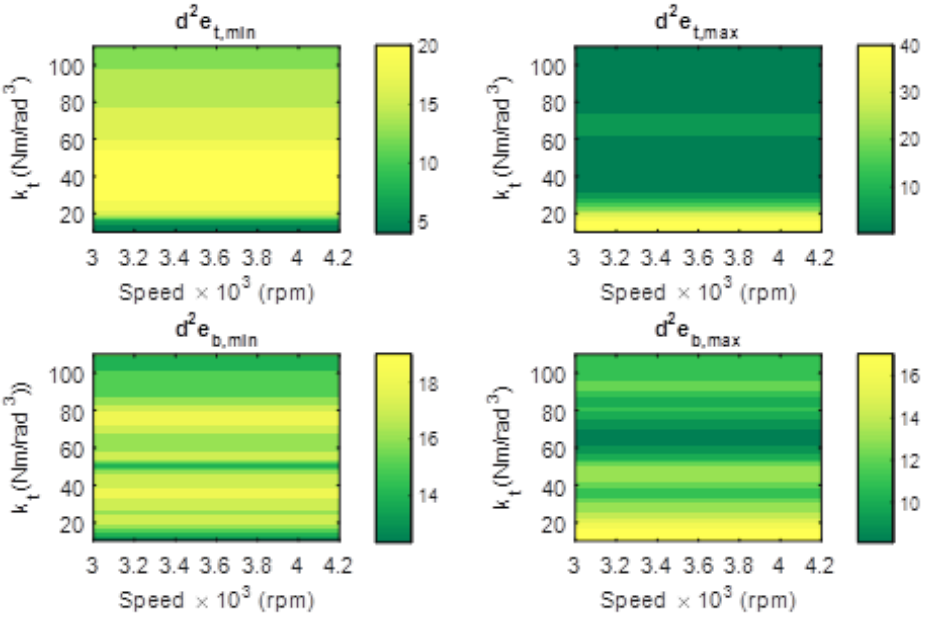

Fig.10. Percentage of variation in eccentricity acceleration amplitudes (impact severity) with absorber stiffness coefficient and engine speed

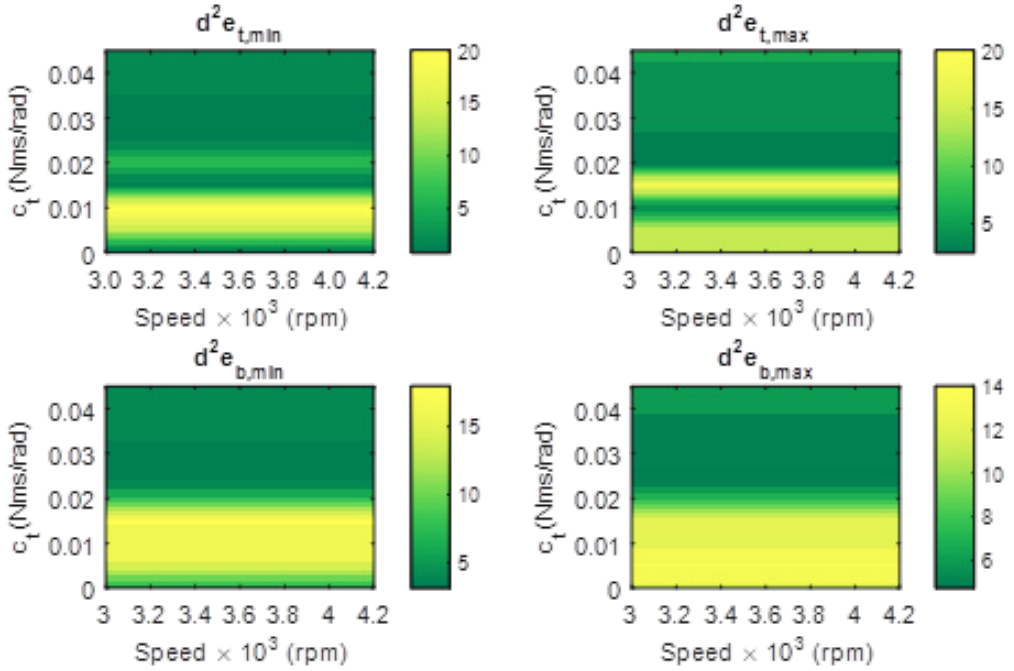

Fig.11. Percentage of variation of eccentricity acceleration amplitudes (impact severity) with absorber damping coefficient and engine speed

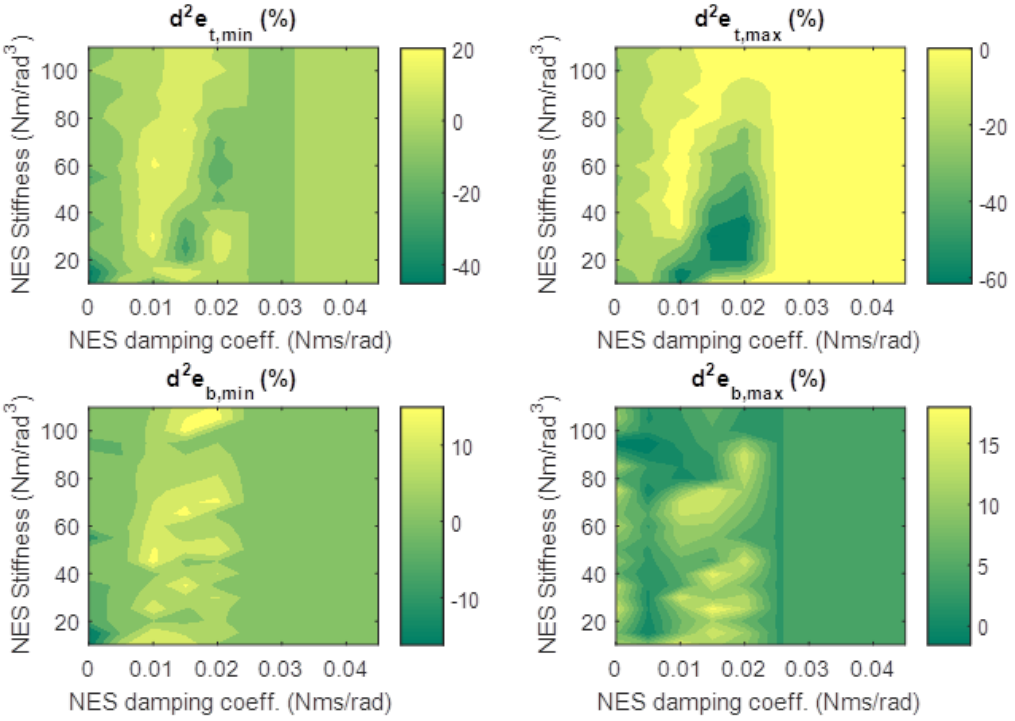

Fig.12. Percentage of variation of eccentricity acceleration amplitudes (impact severity) with absorber damping and stiffness coefficients

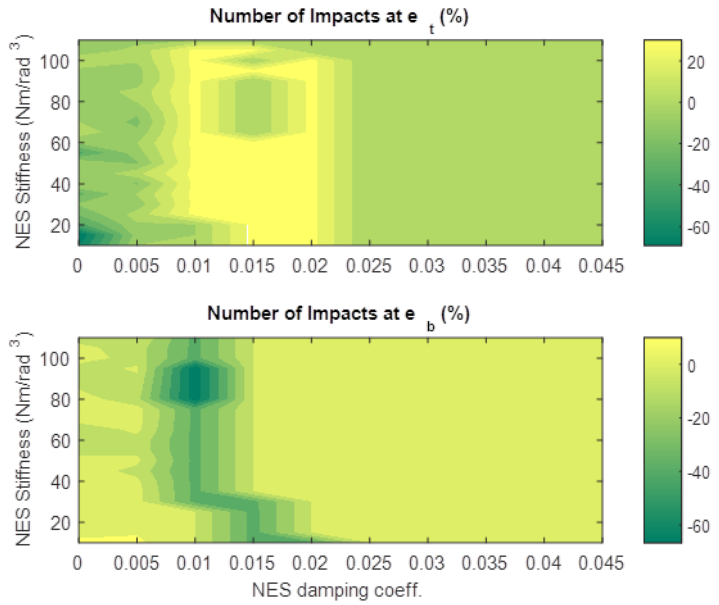

Fig.13. Percentage of variation of impact number with absorber damping and stiffness coefficients

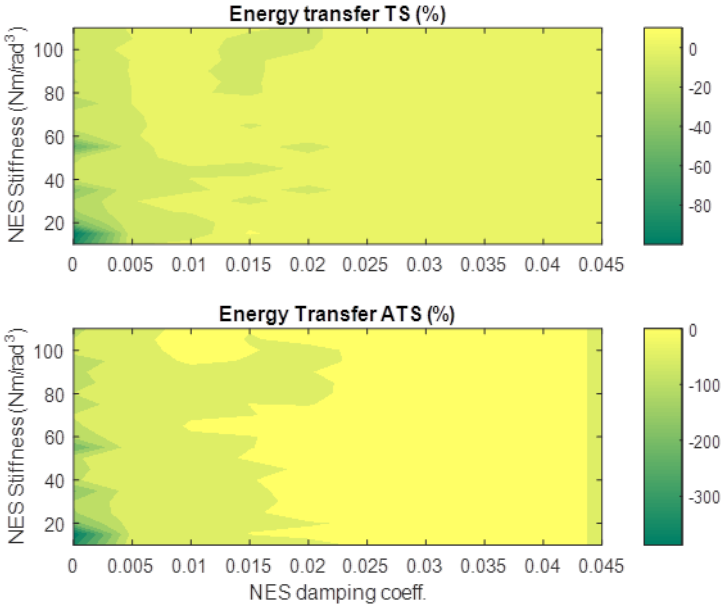

Fig.14. Percentage of variation of energy transfer with absorber damping and stiffness coefficients

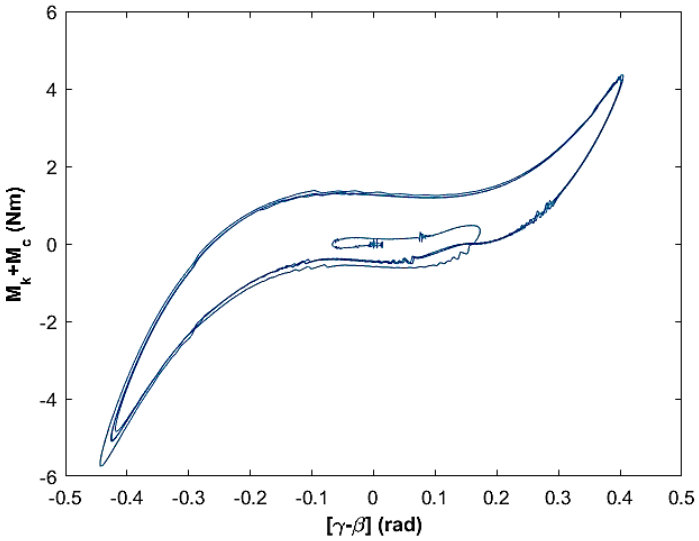

Fig.15. Pendulum absorber hysteresis loop

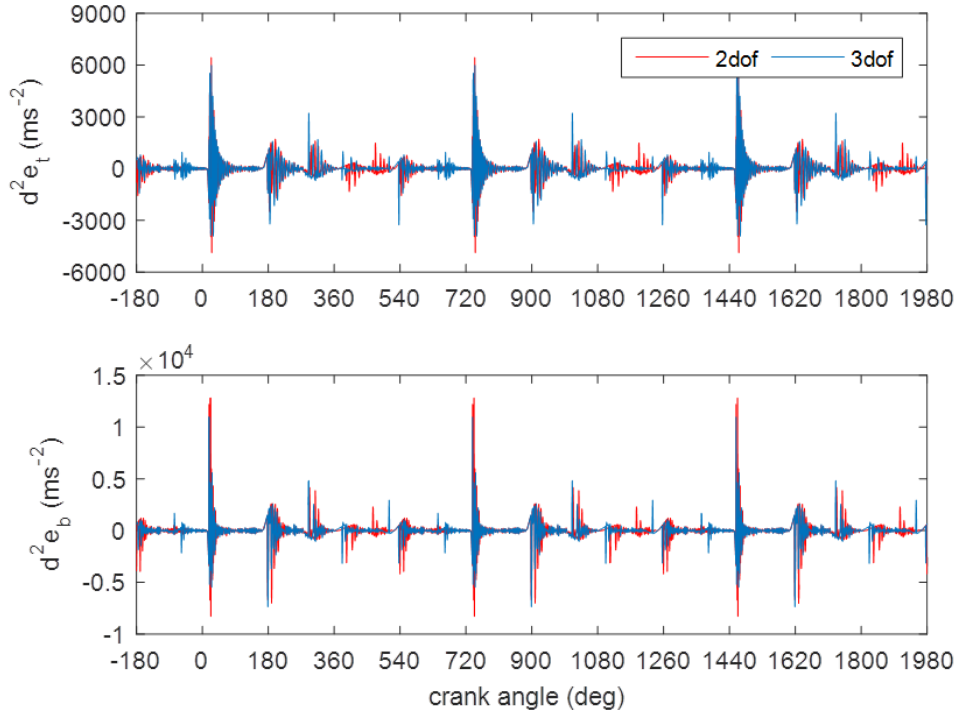

Fig.16. Eccentricity accelerations at the top and bottom of the piston skirt

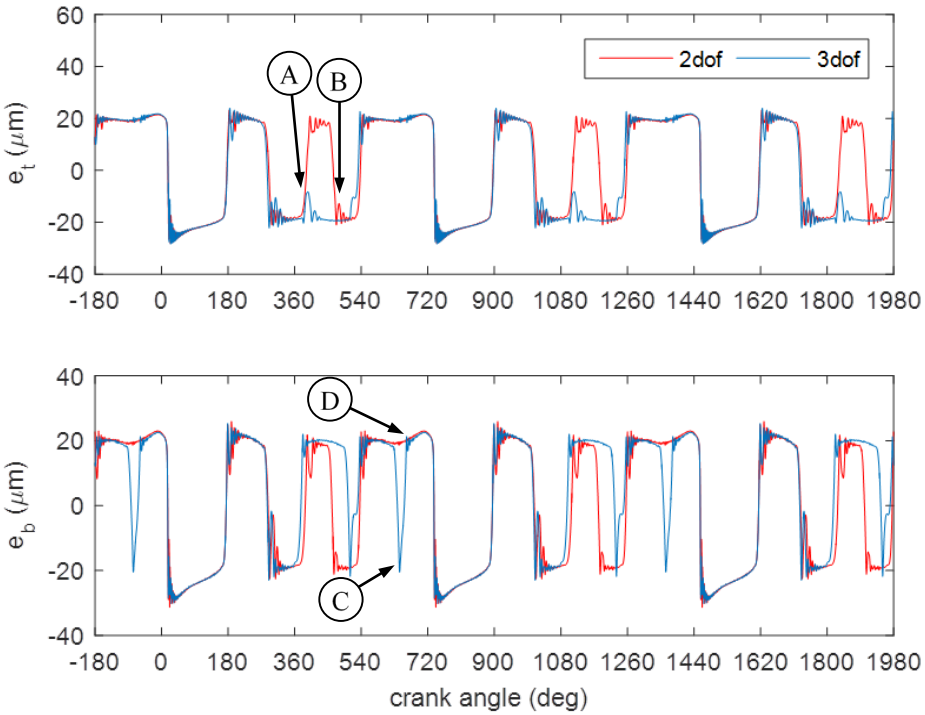

Fig.17. Eccentricity displacements at the top and bottom of the piston skirt

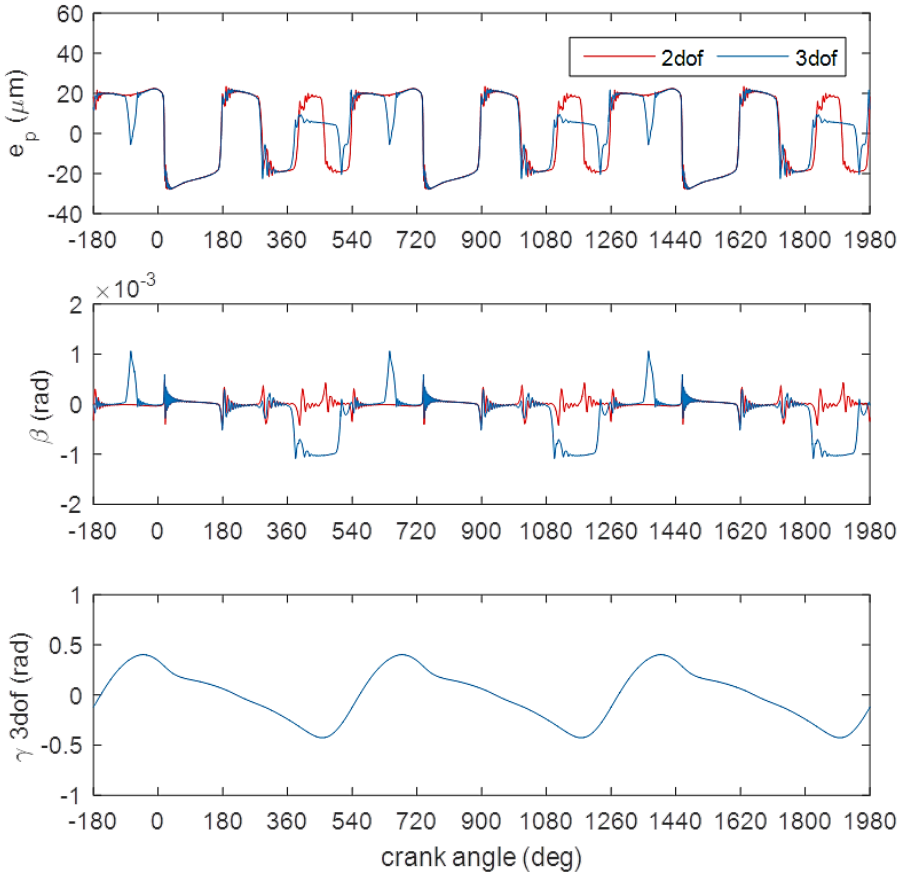

Fig.18. piston secondary motions (translation and rotation) and angular oscillations of pendulum

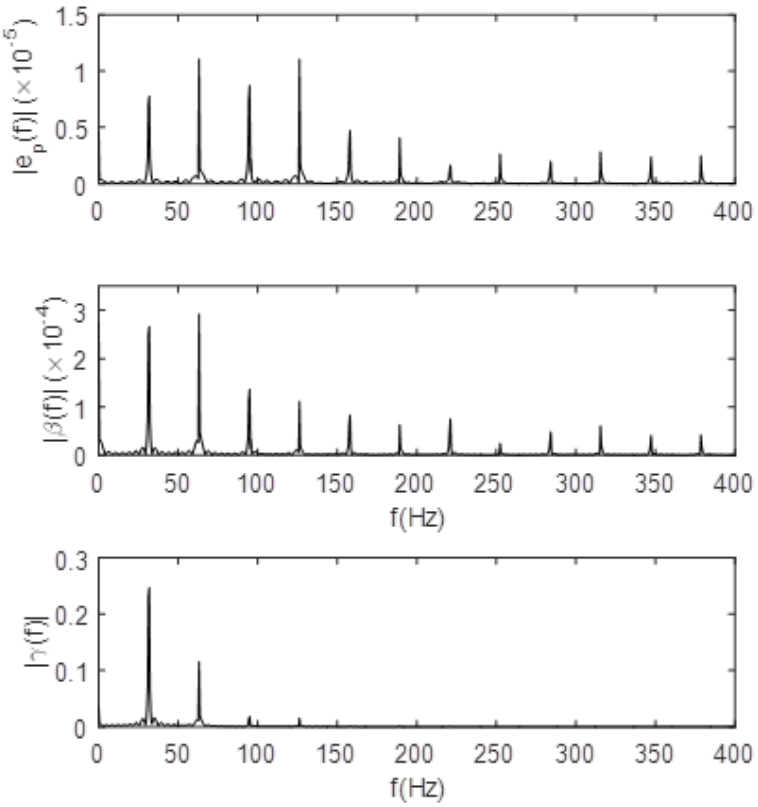

Fig.19. Frequency spectrum of the piston secondary motions and pendulum angular oscillations for 3500rpm engine speed

List of Tables

List of figures

Fig.15. Pendulum absorber hysteresis loop

Fig.16. Eccentricity accelerations at the top and bottom of the piston skirt

Fig.17. Eccentricity displacements at the top and bottom of the piston skirt

Fig.18. piston secondary motions (translation and rotation) and angular oscillations of pendulum

Fig.19. Frequency spectrum of the piston secondary motions and pendulum angular oscillations for 3500rpm engine speed

Table 1. Ranges of values of the system parameters utilised during simulations

Parameter	Value	Unit
$m_{pis} + m_{pin}$	0.25 – 0.4	Kg
m_t	0.125 $(m_{pis} + m_{pin})$	Kg
I_{pis}	$1.5\times10^{-4} - 3\times10^{-4}$	$Kg.m^2$
a	0.015 – 0.03	m
b	0.008 - 0.02	m
L	0.03 – 0.05	m
L_t	0.04 – 0.06	m
k_H	60 – 80	$GN/m^{1.5}$
ζ_H	0.005 – 0.02	--